Nuclear Inst. and Methods in Physics Research, A 989 (2021) 164824

Contents lists available at ScienceDirect

Nuclear Inst. and Methods in Physics Research, A

journal homepage: www.elsevier.com/locate/nima

Performance of neutron spectrum unfolding using deuterated liquid scintillator

M. Febbraro [a,*], B. Becker [b], R.J. deBoer [c,d], K. Brandenburg [e], C. Brune [e], K.A. Chipps [a], T. Danley [e], A. Di Fulvio [f], Y. Jones-Alberty [e], K.T. Macon [c,d], Z. Meisel [e], T.N. Massey [e], R.J. Newby [a], S.D. Pain [a], S. Paneru [e], S. Shahina [c,d], M.S. Smith [a], D. Soltesz [e], S.K. Subedi [e], I. Sultana [e], R. Toomey [g]

[a] Physics Division, Oak Ridge National Laboratory, Oak Ridge, TN, USA
[b] Department of Physics, University of Tennessee, Knoxville, TN, USA
[c] Department of Physics, University of Notre Dame, Notre Dame, IN, USA
[d] The Joint Institute for Nuclear Astrophysics, USA
[e] Department of Physics, Ohio University, Athens, OH, USA
[f] Department of Nuclear Engineering, University of Illinois, Urbana-Champaign, Il, USA
[g] Department of Physics and Astronomy, Rutgers, The State University of New Jersey, Piscataway, NJ, USA

ARTICLE INFO

Keywords:
Neutron spectroscopy
Neutron time-of-flight
Deuterated scintillators
Spectrum unfolding

ABSTRACT

The performance of the maximum likelihood expectation maximization method for unfolding neutron energy spectra using deuterated liquid scintillator is evaluated for future utilization with rare isotope beams. High-resolution neutron energy spectra as well as the detector response matrix were measured at the Edwards Accelerator Laboratory at Ohio University. Maximum-likelihood expectation maximization (MLEM) unfolded neutron spectra are compared with spectra from neutron time-of-flight. The effects of the MLEM stopping criteria and spectrum statistics are also investigated.

1. Introduction

Nuclear reaction measurements with short-lived unstable nuclei pose considerable experimental challenges. Foremost of these challenges are low beam intensities. Their short lifetimes also prevent them from being prepared as accelerator targets and thus must serve as the projectile in reaction measurements. These experiments provide level energy and spectroscopic information needed for nuclear astrophysics and structure studies. Since many transfer and charge exchange reactions of interest are performed on light nuclei (p, d, ^{3}He, ^{4}He), measurements with short-lived unstable nuclei must be performed in inverse reaction kinematics. Inverse reaction kinematics occurs when the mass of the projectile is greater than the mass of the target. This results in a strong neutron-energy dependence with laboratory angle and kinematic compression at forward center-of-mass angles. Fig. 1 shows a comparison of the ^{30}P(d,n)^{31}S reaction in normal and inverse kinematics at $E_{c.m.}$ = 9.375 MeV. Typically, forward center-of-mass angles (<90 degrees, corresponding to backwards laboratory angles) are of interest for measurements astrophysical of importance. In the case of ^{30}P(d,n)^{31}S, this would cover E_n < 10 MeV.

These experimental challenges are further complicated when neutron detection is required. The neutron's lack of charge limits detection schemes to those based on the short-range interaction of the strong force. The most common method for detection of fast neutrons is through elastic scattering reactions, using hydrogen or deuterium. Neutron spectroscopy measurements are typically performed using the neutron time-of-flight (ToF) method where the neutron energy is determined from the ToF of the neutron over a fixed distance. Classically, the neutron energy is given by

$$E_n = \frac{1}{2} m \left(\frac{d}{t} \right)^2, \tag{1}$$

where d is the flight-path distance, t is the time for the neutron to traverse d, and m is the mass of the neutron. The neutron energy resolution (ΔE_n) is given by

$$\left(\frac{\Delta E_n}{E_n} \right)_{ToF} = \sqrt{\left(\frac{2\Delta d}{d} \right)^2 + \left(\frac{2\Delta t}{t} \right)^2}, \tag{2}$$

where Δd is the uncertainty in the flight path distance and Δt is the timing resolution of the system (neutron detector and time-tagged neutron source). Since neutrons can interact anywhere within the detection medium, the uncertainty in the flight path is often largely due to the detector thickness. Typically, the timing resolution is a fixed parameter

* Corresponding author.
E-mail address: febbraromt@ornl.gov (M. Febbraro).

https://doi.org/10.1016/j.nima.2020.164824
Received 19 August 2020; Received in revised form 28 October 2020; Accepted 28 October 2020
Available online 1 December 2020

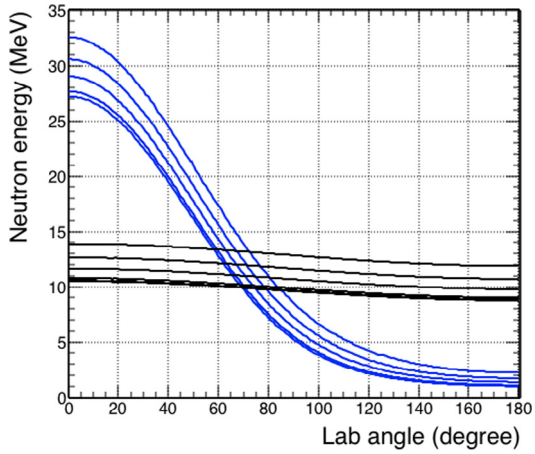

Fig. 1. Comparison of normal (black) and inverse (blue) reaction kinematics for the ^{30}P(d,n)^{31}S reaction at 9.375 MeV center-of-mass. The multiple lines correspond to different final states in ^{31}P. (For interpretation of the references to color in this figure legend, the reader is referred to the web version of this article.)

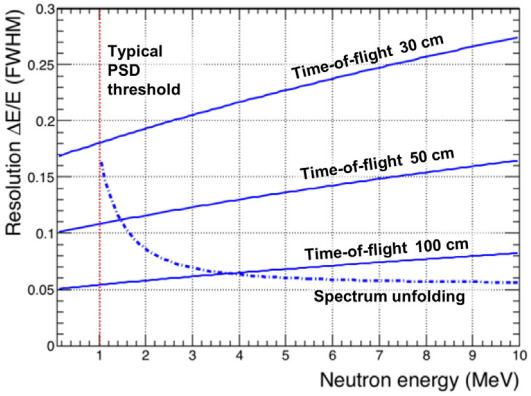

Fig. 2. Comparison of neutron energy resolution extracted from time-of-flight at three distances (solid lines) and spectrum unfolding (dotted line). For the ToF curves, a detector thickness of 5.0 cm and 1.5 ns FWHM timing resolution was used. The vertical red line shows a typical PSD threshold, which serves as a low energy threshold for spectrum unfolding. (For interpretation of the references to color in this figure legend, the reader is referred to the web version of this article.)

limited by the accelerator beam pulse, therefore any improvements in energy resolution must come from an increase in the flight-path distance or from a reduction in detector thickness. Increasing the detector distance leads to a reduction in absolute detection efficiency due to the decrease in solid angle subtended by the detector. Reducing the detector thickness is another option but this adds considerable complexity to the system as more channels are needed to make up for the loss in detector mass and hence detection efficiency.

An alternative approach to measurement of neutron spectra uses spectrum unfolding (SU), a technique that has recently experienced renewed interest in low energy nuclear physics [1–4]. Spectrum unfolding uses detailed knowledge of the relationship between the light and neutron energy response of a detector to unfold a measured spectrum. The relationship between the measured light response spectrum, $\overline{S}$, and the incident neutron energy spectrum, $\overline{x}$, can be modeled in the form of a discrete-form Fredholm integral of the first kind,

$$\overline{S} = \overline{\overline{R}}\,\overline{x}, \tag{3}$$

where $\overline{\overline{R}}$ represents the kernel function, which we will henceforth refer to as the detector response matrix. The success of this approach depends on the condition of $\overline{\overline{R}}$ and the uniqueness of each $\overline{S}_j$ for a given $\overline{x}_i$. The use of enriched deuterium scintillators over those fabricated from natural abundance material enhances this condition [5]. This is primarily due to the asymmetry of the $n + d$ scattering cross section, which produces a characteristic feature (referred to as a recoil peak) in the light spectrum. These peaks are approximately proportional to the incident neutron energy. A neutron energy spectrum can then be extracted by solving for $\overline{x}$ in Eq. (3) using a maximum-likelihood expectation maximization (MLEM) algorithm or other ill-posed inverse problem approaches. Some other examples of unfolding approaches include one-step-late (OSL) method [6], hierarchical Bayesian-MC approach [7], artificial neutral network — least squares approach [8], and maximum entropy [9].

When performing a neutron spectroscopy measurement, the neutron detection method must be chosen according to the requirements of the particular experiment. For instance, a measurement performed at a high-current DC accelerator facility will be limited to the use of SU, as there is no timing information available for ToF. It is also important to consider the energy resolution required for the measurement when comparing methods. Fig. 2 shows a comparison of the energy resolution achievable using SU or ToF at three distances. The vertical dotted line in this figure represents a typical pulse shape discrimination (PSD) threshold, which is related to a detector's ability to discriminate between gamma and neutron events. Below the PSD threshold, SU is not possible due to the inability to distinguish between neutron and gamma events. As neutron energy increases above the PSD threshold, any comparison to ToF resolution must be done as a function of detector distance, timing resolution, and detector thickness. However, for SU, this is not the case as it is independent of flight path or timing.

Fig. 2 demonstrates energy resolution can be maximized over a broad energy range without sacrificing detection efficiency, or signal-to-background ratio, by combining these approaches. The benefit of this is that, for experiments where beam pulsing is possible, which is the case for nearly all RIB facilities, short flight-path ToF can be used to separate beam-related neutrons from background neutrons, while SU can be used to extract high-resolution neutron energy spectra. Data taken with timing provided can be analyzed using both methods offline. Thus, for each measurement, the most appropriate method can be implemented, with the inherent capability of being able to shift to the alternative method to improve the energy resolution as necessary, without the need to modify the experimental configuration.

In this paper, we investigate the performance of neutron spectrum unfolding using a deuterated liquid scintillator detector. A response matrix for this detector was measured along with (d,n) spectra on ^{16}O, ^{2}H, and ^{12}C. We investigate the effect of the stopping criteria on the unfolded spectrum and compare the peak centroids and total counts obtained for analysis of the same data by ToF and SU methods as a function of peak statistics.

2. Experimental setup

Neutron measurements were performed at the Edwards Accelerator Laboratory at Ohio University, utilizing the 30 m neutron ToF tunnel and beam swinger [10]. Neutron spectra were measured using an 73 mm diameter x 50 mm thick ODeSA [11] detector filled with Eljen-315M, which was located at a distance of 8.02(3) m from the reaction target. Data were recorded using a CAEN V1725 250 MS/s, 14-bit waveform digitizer. Details regarding the specific neutron sources used for the response matrix and discrete spectra are provided in the following subsections.

For each event, the waveform was baseline corrected using a continuous moving average filter with threshold and timing information extracted via a constant fraction discrimination method. The PSD parameter, defined as the ratio of the tail integral to the total integral, was determined using a standard charge integration method. A total pulse integral of 400 ns, and a tail integral of 300 ns, which was offset 48 ns from the waveform maximum amplitude, was used for the analysis.

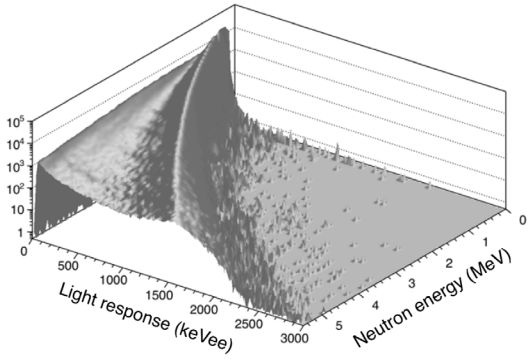

Fig. 3. Response matrix generated using a broad energy neutron source from a thick target ^{nat}Be(d,n) reaction at E_d = 7.00 MeV.

The light response calibration was based on the Compton edge of ^{22}Na, ^{137}Cs, and ^{207}Bi sources, taken at 80% of the edge height. An ^{241}Am source was used as a low-energy calibration point where a 60 keV photo-peak is observed.

To determine the neutron time-of-flight, a Hewlett Packard 8082A pulse generator, triggered by the beam pick-off timing pulse, was used to generate a trapezoidal pulse with a rise time, fall time, and flat top of 40 ns each, matching the sampling frequency of the digitizer. This provides a 10-point leading edge with which a timing resolution of 1.7 ns (FWHM) was achieved via constant fraction discrimination with linear interpolation between points. This timing resolution reflects the accelerator beam pulse width and the relatively large transit-time-spread of the Hamamatsu R6233-100-01 photomultiplier tube used.

2.1. Response matrix

As mentioned, a key ingredient in unfolding a neutron energy spectrum from a measured light response spectrum is the detector response matrix, which we will denote $\overline{\overline{R}}$. The response matrix must span the energy and light response range of the spectra to be unfolded. Looking back at Eq. (3), each column of $\overline{\overline{R}}$ represents the detector response, in measured light output, for a discrete neutron energy. The response matrix is then built up by combining multiple detector responses over an energy range of interest. Experimentally, the response matrix can be measured by stepping through multiple neutron energies and combine these together to form $\overline{\overline{R}}$; however, in practice, this is a very time consuming process. Instead, a more convenient and efficient method for determining $\overline{\overline{R}}$ over a broad energy range is to use a so-called "white" neutron source and extract quasi-monoenergetic neutron energies using ToF. This has its advantages in that the entire matrix is obtained in a single measurement rather than stepping through discrete neutron energies. This was the approach taken for this work. The white neutron source was created by impinging an E_d = 7.00 MeV d$^+$ beam on a thick Be target which resulted in a broad neutron energy distribution [12]. The response matrix was generated by producing a 2D histogram of light response vs. neutron energy calculated from neutron ToF. Fig. 3 shows the measured response matrix with background contributions subtracted using a shadow bar run. Further details regarding determination of the detector response matrix can be found in Ref. [11].

2.2. Discrete neutron spectrum

In addition to the response matrix measurement, the same experimental setup was to measure a high-statistics discrete neutron spectrum for comparing the SU and ToF analysis techniques. The discrete spectrum was created by impinging a 4.0 MeV deuteron beam on a mixed isotope thin solid target which provided discrete neutron spectra

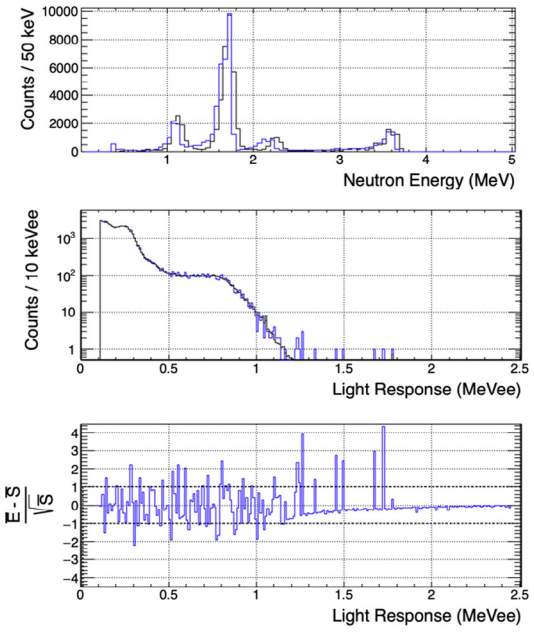

Fig. 4. Unfolded neutron energy spectrum (blue) compared to the same spectrum produced through neutron ToF (black) (top). The light response spectrum (blue) used in the unfolding compared to a estimate spectrum generated by feeding the unfolded spectrum into the forward problem (black) (center). The difference between input spectrum and estimate spectrum over the square root of counts in the input spectrum (bottom). (For interpretation of the references to color in this figure legend, the reader is referred to the web version of this article.)

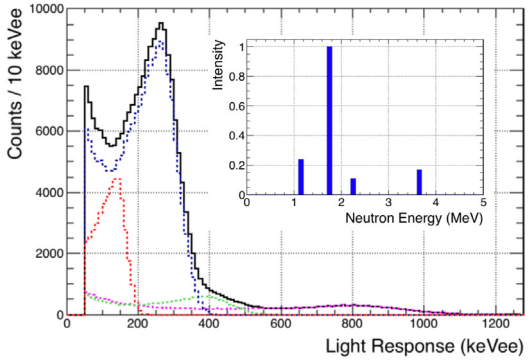

Fig. 5. A simulated light response for a spectrum containing four neutron energies. The solid line shows the total light response while dotted lines represent the individual contributions. The different colors are meant to indicate the different neutron energies.

from the ^{12}C(d,n$_0$), ^{12}C(d,n$_1$), ^{16}O(d,n$_0$), and ^{16}O(d,n$_1$) reactions. This spectrum was taken in the same configuration as the response matrix measurement such that it could be analyzed by both ToF and SU methods.

3. Spectrum unfolding using MLEM

Evaluation of unfolded neutron spectra were performed using the iterative MLEM algorithm [6]. The iterative MLEM algorithm is a Bayesian method which guarantees a local maxima in the expectation value of the likelihood of $\sum_j R_{ij} x_j^{(k)}$ for each bin of s_i. The iterative form of the MLEM algorithm is as follows:

$$x_j^{(k+1)} = \frac{x_j^{(k)}}{\sum_i R_{ij}} \sum_i R_{ij} \frac{s_i}{\sum_l R_{il} x_l^{(k)}}, \tag{4}$$

where s_i is the measured light response spectrum, R_{ij} is the detector response matrix, x_j is the estimate unfolded spectrum, and k is the

iteration number. One complication of the MLEM approach is deciding when the optimum number of iterations has been reached. It has been shown that the level of random noise in the unfolded spectrum increases with the number of iterations [13]. Thus the level of random noise in the unfolded spectrum is dependent on the choice of the stopping criteria. As a stopping criteria, we adapt the MLEM-STOP method [14] that uses an indicator function, which we will denote as $J^{(k)}$, which is constructed by computing the mean squared error of the measured input spectrum S_i and the forward-projected estimate spectrum $q_i^{(k)}$ normalized to the forward-projected mean as follows:

$$q_i^{(k)} = \sum_{j=0}^{J} R_{ij} x_j^{(k)}, \tag{5}$$

$$J^{(k)} = \frac{\sum_{i=0}^{I}(S_i - q_i^{(k)})^2}{\sum_{i=0}^{I} q_i^{(k)}}. \tag{6}$$

As the number of iterations are increased, the unfolded spectrum may arrive at a noise-free condition when the expectation value of the mean-squared deviation between S_i and $q_i^{(k)}$ equals the mean $q_i^{(k)}$. At this point, $J^{(k)} = 1$ and the stopping criteria has been met. In practice, it has been found the algorithm should be terminated just before $J^{(k)} = 1$ [13].

Another consideration is the effect of light response calibration on the extracted neutron spectrum. In the case of neutron spectra which are not statistics limited, ambiguity in the light response calibration does not lead to ambiguity in the peak centroid in the case of ToF as the centroid depends only on the timing. In the case of SU, ambiguity in the light response calibration would lead to ambiguity in the unfolded peak centroid as there would be a difference between the s and R. Above a few MeV, the light response becomes nearly linear, thus ambiguity in the light response calibration is observed as an overall shift in the peak centroid.

A comparison between the discrete neutron data set analyzed by SU and ToF is shown in Fig. 4 (top). A uniform initial estimate spanning the entire unfolding energy range was used. Determination of the ToF spectrum relies only on the measured flight time of the neutron and the flight path distance while SU relies only on the measured light response and is independent of timing. The two are in good agreement not only in energy scale but also intensity. Using the unfolded neutron spectrum, Fig. 4 (middle) also shows a comparison between the forward-projected estimate and the input spectrum. The forward-projected estimate is defined as $\overline{E} = \overline{\overline{R}}\,\overline{x}$, where $\overline{S}$ has been replaced with $\overline{E}$ to denote the projection. The relationship between the measured light response spectrum and unfolded neutron spectrum is illustrated in Fig. 5. Each neutron energy group or peak corresponds to a continuous light response distribution shown as the colored distributions in Fig. 5. The sum of all these distributions makes up the light response spectrum.

The effect of spectrum statistics on the stopping criteria can also be investigated through a comparison of the iteration number obtained by the MLEM-STOP method and the 'ideal' number of iterations. The ideal number of iterations can be determined by minimizing the root-mean-square-error (RMSE) between the unfolded estimate and the ground-truth spectrum, denoted $\overline{x}_j$, as shown in Eq. (7). Since the ToF spectrum is independent of the light response,[1] we take it as the ground-truth spectrum. First scenario is the use the ToF spectrum as the ground-truth spectrum which is shown in Fig. 6. As found in [13], setting the stopping criteria for the indicator function to $J^{(k)} = 1$ tends to over iterate the unfolded spectrum. For this example the minimum occurs at iteration number 266 for the RSME and iteration number 421 for $J^{(k)} = 1$. Fig. 7 shows the change in the total counts in the $\sim$ 3.5 MeV peak as a function of iteration number. The change in peak

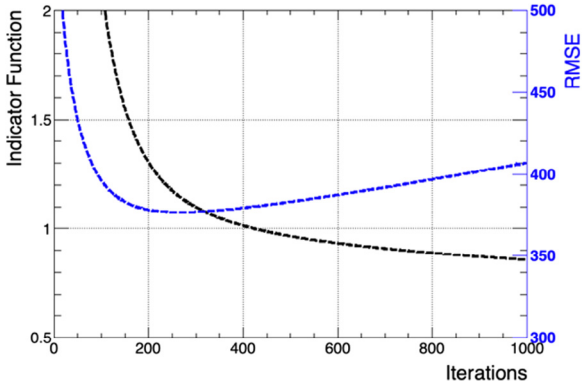

Fig. 6. Comparison between the RMSE (blue) and indicator function (black) with respect to iteration number. The ToF spectrum is taken as the ground-truth spectrum. (For interpretation of the references to color in this figure legend, the reader is referred to the web version of this article.)

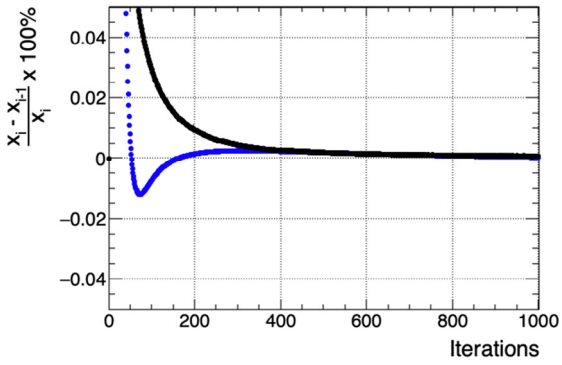

Fig. 7. Percent difference in the unfolded peak counts for the 1.7 MeV (black) and 3.5 MeV (blue) peaks between sequential steps in the iterative MLEM algorithm. The maximum peak counts near iteration number 300 for the 3.5 MeV peak corresponds with the minimum of the RMSE in Fig. 6.

counts quickly becomes sub percent level after 10 s of iterations and also exhibits maximum corresponding to the minimum of the RSME. Likewise, the change in peak counts for the 1.7 MeV peak quickly becomes sub percent level after 10 s of iterations. Thus an over iteration from the 'ideal' number of iterations does not result in a significant change in the final peak counts.

$$RSME = \sqrt{\frac{\sum_{j=0}^{J}(\overline{x}_j - x_j^{(k)})^2}{J}}, \tag{7}$$

4. Stability of the spectrum unfolding

Another important metric is how the unfolded neutron peaks change with spectrum statistics, both in their centroid value and total counts. This is particularly important in the case of RIB experiments, which tend to be statistics limited by low beam intensities. This scenario can be investigated by analyzing a subset of the total data to reduce statistics in $\overline{S}$. There are two interesting cases which we address. Since discrete neutron energies result in continuous light response spectra, due to n-d elastic scattering $\{\theta_n \mid 0 \le \theta_n \le \pi\} \therefore \{E_d(\theta_n) \mid 0 \le E_d(\theta_n) \le 8/9E_n\}$, the light response for lower energies will stack upon higher energies as shown in Fig. 5. The first case we consider is for the highest energy neutrons in the spectrum, where the recoil peak is free from contributions from other neutron energies. The second case we consider is for all other lower energy neutron energies where the entire recoil spectrum in stacked upon higher energy spectra.

To investigate the first case, the peak at ~3.5 MeV shown in Fig. 4 was used. Fig. 8 shows the difference between counts in the unfolded

[1] A threshold of 100 keVee was used for this work which corresponds to $\mathcal{O}(300)$ photons. This assumption may not be true for cases where photon statistics are lower or for detectors which have significant internal reflections.

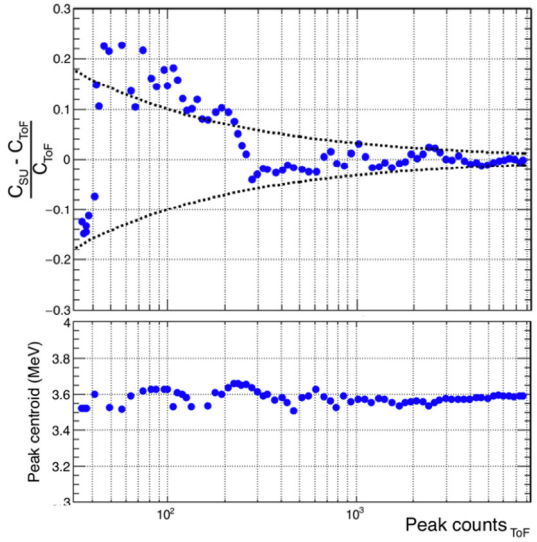

Fig. 8. Difference between neutron counts extracted using spectrum unfolding and ToF methods as a function of total counts (top) in the ~3.5 MeV peak (top). Unfolded peak centroid as a function of total counts (bottom).

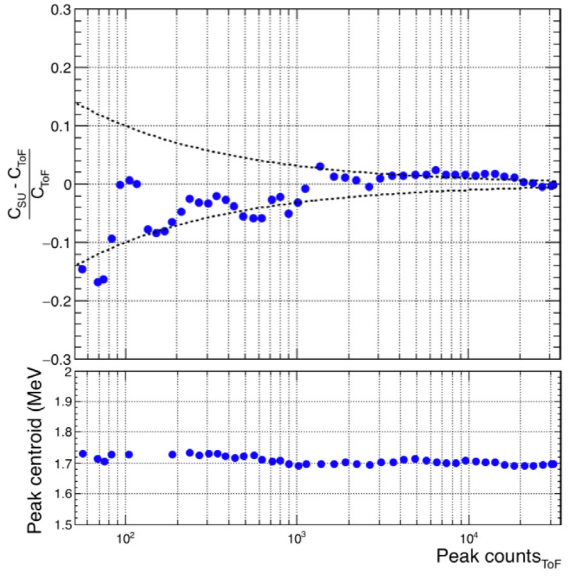

Fig. 9. Difference between neutron counts extracted using spectrum unfolding and ToF methods as a function of total counts in the ~1.7 MeV peak (top). Unfolded peak centroid as a function of total counts (bottom).

spectrum and counts in the same spectrum extracted using ToF for the highest energy peak at ~3.5 MeV. Above a few 1000 counts, the two spectra agree to within ±2%. As the statistics are decreased, the disagreement remains less than $1/\sqrt{N}$ uncertainty above a few 100 counts. At no point between 50–10^4 counts is the difference >25%, or >5% above $1/\sqrt{N}$. The variation in the peak centroid in the unfolded spectrum is <±3% over the range of 50–10^4 counts.

For the second case, the same analysis was performed but for the peak at ~1.7 MeV in Fig. 4. Fig. 9 shows a similar trend to the ~3.5 MeV peak above 1000 counts but follows along the lower $1/\sqrt{N}$ band below 1000 counts. As with the ~3.5 MeV peak, the variation in the peak centroid in the unfolded spectrum is <±3% over the range of 50–10^4 counts. The primary difference between the ~3.5 MeV and the ~1.7 MeV being that the ~1.7 MeV peak has contributions from the two higher peaks. These plots illustrate the robustness of the spectrum unfolding approach in extracting neutron energy spectra down to a few 100 counts.

5. Conclusion

The performance of spectrum unfolding using a deuterated liquid scintillator using the iterative MLEM algorithm was shown. The MLEM-STOP method was shown to be sufficient as a stopping criteria for the MLEM algorithm. A comparison between a neutron spectrum analyzed using SU and neutron ToF as a function of spectrum statistics was performed. The extracted neutron spectra agree to <10% above a few hundred counts which makes this technique suitable for RIB experiments. The variation in the peak centroid in the unfolded spectrum is <±3% over the range of 50–10^4 counts. These results demonstrate the performance and stability of spectrum unfolding approach to extract neutron energy spectra using deuterated liquid scintillators.

CRediT authorship contribution statement

M. Febbraro: Conceptualization, Methodology, Formal analysis, Writing - original draft. **B. Becker:** Investigation. **R.J. deBoer:** Conceptualization, Writing - original draft. **K. Brandenburg:** Investigation. **C. Brune:** Investigation. **K.A. Chipps:** Conceptualization. **T. Danley:** Investigation. **A. Di Fulvio:** Writing - original draft. **Y. Jones-Alberty:** Investigation. **K.T. Macon:** Investigation, Writing - original draft. **Z. Meisel:** Investigation. **T.N. Massey:** Investigation. **R.J. Newby:** Investigation. **S.D. Pain:** Investigation, Conceptualization. **S. Paneru:** Investigation. **S. Shahina:** Writing - original draft. **M.S. Smith:** Writing - original draft. **D. Soltesz:** Investigation. **S.K. Subedi:** Investigation. **I. Sultana:** Investigation. **R. Toomey:** Investigation, Writing - original draft.

Declaration of competing interest

The authors declare that they have no known competing financial interests or personal relationships that could have appeared to influence the work reported in this paper.

Acknowledgments

We gratefully thank the staff of the Ohio University Edwards Accelerator Laboratory for their assistance with experimental setup and operation of the accelerator. This material is based upon work supported by the U.S. Department of Energy, Office of Science, Office of Nuclear Physics, under Award Number DE-AC05-00OR22725. RJD, KTM, and SS were supported by the National Science Foundation through Grant No. Phys-0758100 and the Joint Institute for Nuclear Astrophysics through Grant No. Phys-0822648 and PHY-1430152 (JINA Center for the Evolution of the Elements. OU support was provided by U.S. Department of Energy under Grants No. DE-FG02-88ER40387, No. DE-NA0003909, and DE-SC0019042.)

References

[1] M. Febbraro, C. Lawrence, H. Zhu, B. Pierson, R. Torres-Isea, F. Becchetti, J. Kolata, J. Riggins, Deuterated scintillators and their application to neutron spectroscopy, Nucl. Instrum. Methods Phys. Res. A 784 (2015) 184–188, Symposium on Radiation Measurements and Applications 2014 (SORMA XV).

[2] M. Febbraro, F. Becchetti, R. Torres-Isea, J. Riggins, C. Lawrence, J. Kolata, A. Howard, (d,n) Proton-transfer reactions on ^{9}Be, ^{11}B, ^{13}C, ^{14,15}N, and ^{19}F and spectroscopic factors at $E_d = 16$ MeV, Phys. Rev. C 96 (2017) 024613.

[3] Q. Liu, M. Febbraro, R.J. deBoer, A. Boeltzig, Y. Chen, C. Cerjan, M. Couder, B. Frentz, J. Görres, E.A. Henry, E. Lamere, K.T. Macon, K.V. Manukyan, L. Morales, P.D. O'Malley, S.D. Pain, W.A. Peters, D. Schneider, C. Seymour, G. Seymour, E. Temanson, R. Toomey, B.V. Kolk, J. Weaver, M. Wiescher, Measurement of the ^{10}B$(\alpha, n_0)^{13}$N cross section for 2.2 < E_α < 4.9 MeV and its application as a diagnostic at the National Ignition Facility, Phys. Rev. C 100 (2019) 034601.

[4] Q. Liu, M. Febbraro, R.J. deBoer, S. Aguilar, A. Boeltzig, Y. Chen, M. Couder, J. Görres, E. Lamere, S. Lyons, K.T. Macon, K. Manukyan, L. Morales, S. Pain, W.A. Peters, C. Seymour, G. Seymour, R. Toomey, B.V. Kolk, J. Weaver, M. Wiescher, Low-energy cross-section measurement of the $^{10}B(\alpha, n)^{13}N$ reaction and its impact on neutron production in first-generation stars, Phys. Rev. C 101 (2020) 025808.

[5] C.C. Lawrence, A. Enqvist, M. Flaska, S.A. Pozzi, F.D. Becchetti, Comparison of spectrum-unfolding performance of (EJ315) and (EJ309) liquid scintillators on measured ^{252}Cf pulse-height spectra, Nucl. Instrum. Methods Phys. Res. A 729 (2013) 924–929.

[6] B. Pehlivanovic, S. Avdic, P. Marinkovic, S. Pozzi, M. Flaska, Comparison of unfolding approaches for monoenergetic and continuous fast-neutron energy spectra, Radiat. Meas. 49 (2013) 109–114.

[7] H. Zhu, Y. Altmann, A.D. Fulvio, S. McLaughlin, S. Pozzi, A. Hero, A hierarchical Bayesian approach to neutron spectrum unfolding with organic scintillators, IEEE Trans. Nucl. Sci. 66 (10) (2019) 2265–2274.

[8] S.A. Hosseini, Neutron spectrum unfolding using artificial neural network and modified least square method, Radiat. Phys. Chem. 126 (2016) 75–84.

[9] M. Reginatto, P. Goldhagen, Maxed, a computer code for maximum entropy deconvolution of multisphere neutron spectrometer data, Health Phys. 77 (5) (1999) 579–583.

[10] Z. Meisel, C.R. Brune, S.M. Grimes, D.C. Ingram, T.N. Massey, A.V. Voinov, The Edwards Accelerator Laboratory at Ohio University, Physics Procedia 90 (2017) 448–454.

[11] M. Febbraro, R. Toomey, S. Pain, K. Chipps, B. Becker, R. Newby, Z. Meisel, T. Massey, C. Brune, Q. Liu, R. deBoer, K. Macon, A. Boeltzig, J. O'Neill, M. Smith, M. Wiescher, D. Soltesz, I. Sultana, K. Brandenburg, S. Subedi, S. Paneru, T. Danley, Y. Alberty-Jones, The ORNL Deuterated Spectroscopic Array – odesa, Nucl. Instrum. Methods Phys. Res. A 946 (2019) 162668.

[12] W.B. Howard, S.M. Grimes, T.N. Massey, S.I. Al-Quraishi, D.K. Jacobs, C.E. Brient, J.C. Yanch, Measurement of the thick-target $^{9}be(p,n)$ neutron energy spectra, Nucl. Sci. Eng. 138 (2) (2001) 145–160.

[13] L. Montgomery, A. Landry, G.A. Makdessi, F. Mathew, J. Kildea, A novel mlem stopping criterion for unfolding neutron fluence spectra in radiation therapy, Nucl. Instrum. Methods Phys. Res. A 957 (2020) 163400.

[14] F.B. Bouallègue, J. Crouzet, D. Mariano-Goulart, A heuristic statistical stopping rule for iterative reconstruction in emission tomography, Ann. Nucl. Med. 27 (2013) 84–95.